View metadata, citation and similar papers at core.ac.uk

brought to you by CORE

provided by Purdue E-Pubs

Purdue University
Purdue e-Pubs

Birck and NCN Publications | Birck Nanotechnology Center

8-1-2011

Covalent attachment of a peptide to the surface of gallium nitride

Matthew S. Makowski
Purdue University, mmakowsk@purdue.edu

Dmitry Y. Zemlyanov
Birck Nanotechnology Center, Purdue University, dimazemlyanov@purdue.edu

Jason A. Lindsey
Purdue University

Jonathan C. Bernhard
Purdue University, jcbernha@purdue.edu

Evan M. Hagen
Purdue University

See next page for additional authors

Follow this and additional works at: http://docs.lib.purdue.edu/nanopub

Part of the Nanoscience and Nanotechnology Commons

Makowski, Matthew S.; Zemlyanov, Dmitry Y.; Lindsey, Jason A.; Bernhard, Jonathan C.; Hagen, Evan M.; Chan, Burke K.; Petersohn, Adam A.; Medow, Matthew R.; Wendel, Lindsay E.; Chen, Dafang F.; Canter, Jamie M.; and Ivanisevic, Albena, "Covalent attachment of a peptide to the surface of gallium nitride" (2011). *Birck and NCN Publications.* Paper 978.
http://docs.lib.purdue.edu/nanopub/978

This document has been made available through Purdue e-Pubs, a service of the Purdue University Libraries. Please contact epubs@purdue.edu for additional information.

Authors
Matthew S. Makowski, Dmitry Y. Zemlyanov, Jason A. Lindsey, Jonathan C. Bernhard, Evan M. Hagen, Burke K. Chan, Adam A. Petersohn, Matthew R. Medow, Lindsay E. Wendel, Dafang F. Chen, Jamie M. Canter, and Albena Ivanisevic

This article is available at Purdue e-Pubs: http://docs.lib.purdue.edu/nanopub/978

Surface Science 605 (2011) 1466–1475

Contents lists available at ScienceDirect

Surface Science

journal homepage: www.elsevier.com/ locate/susc

Covalent attachment of a peptide to the surface of gallium nitride

Matthew S. Makowski [a], Dmitry Y. Zemlyanov [b], Jason A. Lindsey [a], Jonathan C. Bernhard [a], Evan M. Hagen [a], Burke K. Chan [a], Adam A. Petersohn [a], Matthew R. Medow [a], Lindsay E. Wendel [a], Dafang Chen [a], Jamie M. Canter [a], Albena Ivanisevic [a,c,*]

[a] Weldon School of Biomedical Engineering, Purdue University, West Lafayette, IN, 47907, United States
[b] Birck Nanotechnology Center, Purdue University, West Lafayette, IN, 47907, United States
[c] Department of Chemistry, Purdue University, West Lafayette, IN, 47907, United States

ARTICLE INFO

Article history:
Received 27 October 2010
Accepted 13 May 2011
Available online 23 May 2011

Keywords:
Olefin cross metathesis
Gallium nitride
Surface functionalization
Grubbs catalysis
Semiconductor
X-ray photoelectron spectroscopy

ABSTRACT

The properties of GaN have made it not only an ideal material for high power and high frequency electronic devices, but also a semiconductor suitable for application in biosensing devices. The utilization of GaN in electronic biosensors has increased the importance of characterizing robust and easily implemented organic functionalization methods for GaN surfaces. This work demonstrates and characterizes a route to functionalize the GaN (0001) surface with two organic molecules, hexylamine and a peptide, through olefin cross-metathesis with Grubbs first generation catalyst. The GaN (0001) surface was chlorinated, functionalized with a terminal alkene group using a Grignard reaction, and then terminated with a carboxyl group using an olefin cross-metathesis reaction. With a condensation reaction, the final step in the reaction scheme bound hexylamine or a peptide to the carboxyl terminated GaN surface. Qualitative and quantitative X-ray photoelectron spectroscopy (XPS) data verified the success of each step in the reaction scheme. Surface element composition, adlayer coverages, and adlayer thicknesses were calculated based on the XPS data. At least a monolayer of surface molecules covered the GaN surface.

© 2011 Elsevier B.V. All rights reserved.

1. Introduction

In addition to the capability of GaN devices to operate in high temperature, high power, and high frequency applications [1–3], GaN is also an important semiconductor material for biological sensing devices due to its biocompatibility [4,5], chemical stability [3,6], and the ability to bind ligands to the Ga-polar face of the wurtzite crystal structure [4].

Many studies have demonstrated the application of GaN biosensing devices. One type of highly sensitive GaN biosensor structure is the AlGaN/GaN high electron mobility transistor (HEMT). In these devices the piezoelectric and spontaneous polarizations at the AlGaN/GaN heterojunction induce a channel with high charge carrier mobility [7]. Due to the close proximity of this channel to the device surface, the binding of charged biological analytes at the surface is detected by modulation of channel resistance [8]. Demonstrated biosensing applications of the AlGaN/GaN HEMTs include detection of ions [9], metabolites [10,11], proteins [12–17], pathogens [18], toxins [19], DNA hybridization [20], and extracellular electrical activity [21,22]. Despite the prevalence of the thin-film AlGaN/GaN structures in GaN biosensors, GaN nanowire (NW) devices are also useful in biosensing applications [23]. The applications of GaN NWs in biosensing include detection of DNA hybridization and DNA mutations [24,25].

In biosensing applications semiconductor surface functionalization is important for several reasons. Functionalization passivates the surface before exposure to aqueous environments, controls charge transport across the surface, and decreases nonspecific protein adsorption [26–28]. The literature demonstrates GaN surface functionalizations in both vacuum and ambient conditions. Bermudez conducted a variety of GaN surface functionalization techniques in ultra high vacuum by binding a variety of molecules that include water, ammonia, aniline, and 1-octanethiol [29–36]. Additional GaN surface studies performed under vacuum conditions include binding of amines and removing surface contamination [37,38]. Surface functionalizations achieved under ambient conditions include binding organophosphonic acids to the surface oxide of GaN and binding alkene molecules directly to the GaN surface with ultraviolet photopatterning [39–41]. Many of the AlGaN/GaN HEMT biosensors do not have the AlGaN surfaces directly functionalized with covalently bound organic molecules. Instead, the gate surface is modified by the growth of an oxide [17], the deposition of gold [9,16,18], the physisorption of extracellular matrix proteins [21,22], or the growth of nanorods [10,11]. Specificity for analyte detection is achieved by functionalizing the layer covering the AlGaN layer.

One method of direct covalent functionalization of semiconductor surfaces is through olefin metathesis. In olefin metathesis, C – C bonds

* Corresponding author at: Weldon School of Biomedical Engineering, Purdue University, West Lafayette, IN, 47907, United States. Tel.: +1 765 496 3676; fax: +1 765 496 1459.
E-mail address: albena@purdue.edu (A. Ivanisevic).

0039-6028/$ – see front matter © 2011 Elsevier B.V. All rights reserved.
doi:10.1016/j.susc.2011.05.015

are formed as a result of alkenes interchanging alkylidene functional groups through a transition metal-catalyzed reaction [42–44]. The ruthenium-based olefin metathesis catalysts are stable in various solvents, work with a variety of functional groups, and are optimized for diverse applications [42–46]. Several studies have demonstrated the use of these catalysts to functionalize silicon surfaces through olefin metathesis [47–50].

The work presented here demonstrates the application of olefin cross-metathesis to functionalize the surface of GaN (0001) with a carboxyl group for subsequent peptide binding. The work presented here expands on the initial demonstration of olefin metathesis on GaN performed in this laboratory [51]. Similar to work done on silicon and gallium phosphide, the GaN surface was first terminated with hydrogen atoms, activated by chlorination, and then terminated with an alkene group via a Grignard reaction [49,50,52]. An olefin cross-metathesis reaction with Grubbs first generation catalyst, a ruthenium-based olefin metathesis catalyst, was used to functionalize the GaN surface with a terminal carboxyl group. Lastly, a peptide was bound to the surface by a condensation reaction. X-ray photoelectron spectroscopy (XPS) was used to analyze the surface following each reaction step.

2. Materials and methods

2.1. Materials and chemicals

The GaN (0001) used in this work was undoped and grown on a sapphire substrate. The hydrochloric acid, acetone, tetrahydrofuran (99%), and dichloromethane (99.9%) were purchased from Mallinckrodt. The chlorobenzene (99.8%), benzoyl peroxide, 2M allylmagnesium chloride in tetrahydrofuran, Grubbs first generation catalyst, 6-heptenoic acid (99%), hexylamine (99%), and phosphorus pentachloride (≥98%) were purchased from Sigma Aldrich. 2-(N-Morpholino) ethanesulfonic acid (MES) (>99%) was purchased from Amresco. 1-ethyl-3-[3-dimethylaminopropyl]carbodiimide hydrochloride (EDC) was purchased from Thermo Scientific. All chemicals were used as received. All water was from a Millipore Milli-Q Synthesis A10 System.

2.2. Wafer preparation

GaN wafers were cut into approximately 3 mm × 3 mm squares using a diamond-tipped scribe. The cut wafers were rinsed sequentially with acetone, ethanol, and water. The wafers were then etched in 11.65 M HCl at room temperature for 5 min to remove the surface oxide. The wafers were then rinsed sequentially with water, ethanol, and dried with nitrogen gas. Following the wafer preparation steps and between subsequent processing steps, the GaN wafers were stored in a vacuum desiccator to decrease the rate of oxide formation.

2.3. Hydrogen termination

To terminate the surface gallium atoms with hydrogen, a SEOCAL 5200S microwave plasma chemical vapor deposition system was used to generate hydrogen plasma at a power of 10 W. The GaN wafers were exposed to the hydrogen plasma for 10 min in an environment of 95% argon and 5% hydrogen at a total pressure of 53 Pa.

2.4. Chloride termination

The chloride termination and all subsequent reactions through the olefin cross-metathesis reaction were conducted in a nitrogen-purged glove box. 1.14 g of phosphorus pentachloride was added to 10 mL of chlorobenzene to create a saturated solution. A few crystals of benzoyl peroxide were added as a free radical initiator. The GaN wafers were then submerged in the chlorobenzene solution. The solution was continuously stirred, heated, and maintained at 92 °C for 30 min. The GaN wafers were washed extensively with chlorobenzene, rinsed with ethanol, dried with nitrogen gas, and stored in a vacuum desiccator.

2.5. Alkene termination

The alkene termination and all subsequent reactions through the olefin cross-metathesis reaction were performed with the GaN wafers placed within the reaction wells of a fluidic device composed of polyetheretherketone (PEEK) as shown in Fig. 1. The fluidic device was placed in a nitrogen-purged glove box. Two 1 mL glass syringes (1001 TLL, Hamilton Company) were connected to the fluid ports on the fluidic device. 1.8 mL of 2M allylmagnesium chloride in tetrahydrofuran (THF) was infused into the fluidic system composed of the syringes and fluidic device. A syringe pump (NE-1000, New Era Pump Systems) was used to maintain a continuous flow of solution through the fluidic device and over the wafer surfaces. The solution was heated and maintained at 60 °C for 30 min. After cooling for several minutes, 1.5 mL of pure THF was pumped through the fluidic device for 30 min to remove surface precipitate. Each wafer was soaked in 0.5 mL THF overnight to further dissolve the surface precipitate. The wafers were rinsed with ethanol, dried with nitrogen gas, and stored in a vacuum desiccator.

2.6. Olefin cross-metathesis

The GaN wafers were placed in the fluidic device within the nitrogen-purged glove box. A solution of 18.4 mg of Grubbs first generation catalyst in 1.5 mL of dichloromethane was infused into the fluidic system. The syringe pump was connected to maintain solution flow over the wafer surfaces. The solution was heated and maintained at 40 °C for 30 min. After several minutes of cooling, the solution was drained from the fluidic device and 1.8 mL of dichloromethane was infused and pumped through the fluidic device for 30 min to remove any unbound catalyst. The fluidic device was then flushed with ethanol and dried with nitrogen gas. A solution of 242 μL of 6-heptenoic acid in 1.8 mL of dichloromethane was then infused into the fluidic system. The syringe pump was connected to maintain solution flow over the wafer surfaces. The solution was heated and maintained at 40 °C for 2 h. After cooling, 1.8 mL of pure dichloromethane was pumped through the fluidic device for 30 min to remove any unbound 6-heptenoic acid. The wafers were rinsed with ethanol, dried with nitrogen gas, and placed in a vacuum desiccator.

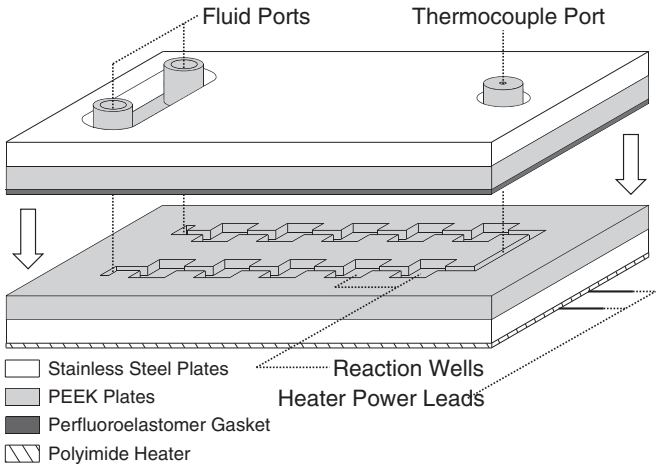

Fig. 1. Schematic of the fluidic device that contained the GaN wafers in the reaction wells during surface functionalization. The two stainless steel plates are clamped together to bring the perfluoroelastomer gasket into contact with the lower PEEK plate.

2.7. Amine conjugation

Two carboxyl-terminated GaN wafers were each placed in a microcentrifuge tube with 700 μL of 0.1 M MES buffer. 1.52 μL of hexylamine was added to one microcentrifuge tube, and 2.2 mg of peptide was added to the other microcentrifuge tube. The peptide sequence was NYQWVPYQGRVPYPRPGTC with the carboxyl terminus replaced with an amide so that the only carboxyl available for the conjugation reaction was the carboxyl group terminating the GaN surface. A solution of 10.3 mg of EDC in 1 mL Milli-Q water was prepared. A volume of 100 μL of this EDC solution was added to each microcentrifuge tube. The microcentrifuge tubes were placed on a rocking platform for 3 h during the conjugation reaction. The wafers were then washed with Milli-Q water, dried with nitrogen gas, and placed in a vacuum desiccator.

2.8. X-ray photoelectron spectroscopy

All XPS data was collected by a Kratos Axis Ultra DLD spectrometer using Al Kα radiation of 1486.6 eV at pass energy of 20 eV for high resolution spectra. The spectra were collected at 0, 45, and 60° from the surface normal. Charge neutralization was accomplished with a commercial Kratos charge neutralizer. All data analysis was performed with CasaXPS software version 2.3.12 (www.casaxps.com). Prior to data analysis, the N 1s peak of GaN was set to a binding energy of 397.00 eV to correct for charge on each sample. C 1s peaks were not used for charge correction since the adsorbed carbon species gave more variability when charge correction was attempted with the C 1s peaks. Peak fitting was performed following a linear or Shirley background subtraction. Curve fitting was achieved with Gaussian/Lorentzian peak shapes to identify contributions from overlapping atomic or chemical species.

3. Calculations

To quantitatively compare the composition of surface species on the GaN wafers following each step in the scheme, the percentages of surface atomic species were calculated according to the following equation:

$$atomic\,\%\ of\ element\ i = 100\frac{\frac{S_i}{(RSF_i)(T_i)(MFP_i)}}{\sum_j \frac{S_j}{\left(RSF_j\right)\left(T_j\right)\left(MFP_j\right)}} \quad (1)$$

where S_i is the area of i-th photoemission peak, RSF_i is the corresponding relative sensitivity factor, T_i is a spectrometer transmission function for the specific kinetic energy, and MFP is the correction for inelastic mean free path of the photoelectron. This model assumes a homogeneous distribution of elements in the near surface region. The element compositions calculated using Eq. (1) are shown in Table 1.

Coverage of the GaN (0001) surface was calculated following each step of the reaction scheme. Coverage was defined as the ratio of the number of bound surface molecules to the number of surface gallium atoms. A non-attenuating adlayer approximation described by Fadley was used to calculate surface coverage [54]. This approach was demonstrated in a number of examples [55–59]. The adlayer coverage, Θ, is approximated by the following simplified equation:

$$\Theta = \frac{N_l(\theta)}{N_s(\theta)}\frac{\frac{d\sigma_s}{d\Omega}}{\frac{d\sigma_l}{d\Omega}}\frac{\Lambda_e^{subst}(E_s)\cdot\ cos\ \theta}{d} \quad (2)$$

where $N_l(\theta)$ and $N_s(\theta)$ are the intensities (areas) of the photoemission peaks of the adlayer and substrate, respectively. The terms $d\sigma_s/d\Omega$ and $d\sigma_l/d\Omega$ represent the subshell differential cross-sections and account for the Scofield cross-section and a correction factor based on the Reilman asymmetric parameter for the substrate and adlayer, respectively. Λ_e^{subst} represents the effective electron attenuation length (EAL) of the photoelectrons emitted from the substrate while traveling within the substrate. θ represents the photoemission angle measured between surface normal and the axis of an energy analyzer. The d term represents the distance between adjacent layers of gallium atoms in the GaN (0001) substrate. For this work, d equal to 5.185 Å was used. To simplify Fadley's original equation, equality of the adlayer and substrate values of acceptance solid angle and effective specimen area were assumed. Results of the coverage calculations are displayed in Tables 4 and 5.

Since the non-attenuating adlayer approximation does not hold true for a thick adlayer, for instance a peptide layer, an attenuating layer approximation by Fadley [54] was used. The photoelectron intensity from a bare substrate, $Ns^0(\theta)$, and the intensity from a substrate covered by a uniform adlayer of thickness t, $Ns(\theta)$, can be written as:

$$N_s^0(\theta) = I_0\Omega_0(E_s)A_0(E_s)D_0\rho_{subst}\frac{d\sigma_s}{d\Omega}\Lambda_e^{subst}(E_s)\ cos\ \theta \quad (3)$$

$$N_s(\theta) = I_0\Omega_0(E_s)A_0(E_s)D_0\rho_{subst}\frac{d\sigma_s}{d\Omega}\Lambda_e^{subst}(E_s)\ cos\ \theta\ exp\left(\frac{-t}{\Lambda_e^{adlayer}(Es)\ cos\ \theta}\right). \quad (4)$$

Taking the ratio of the intensity of the substrate covered by a uniform adlayer, $N_s(\theta)$, to the intensity of a bare substrate, $N_s^0(\theta)$, by dividing Eq. (4) by Eq. (3) gives Eq. (5)[55,60].

$$\frac{N_s(\theta)}{N_s^0(\theta)} = exp\left(\frac{-t}{\Lambda_e^{adlayer}(E_s)\ cos\ \theta}\right) \quad (5)$$

where $\Lambda_e^{adlayer}(E_s)$ is the attenuation length of a photoelectron from the substrate through the adlayer, and θ is the angle between surface normal and the direction of photoelectron emission. When plotting $\ln[N_s(\theta)/N_s^0(\theta)]$ versus $1/cos\theta$ the resulting slope is $-t/\Lambda_e^{adlayer}(E_s)$. Use of this graphic method to determine adlayer thickness gives more accurate results than using a single ratio of intensities [55]. This method was used to calculate the adlayer thicknesses in the first two data columns in Table 6.

Table 1
Surface element composition.

	C	Ca	Cl	Ga	Mg	N	O	Ru
HCl etched	11.9	–	1.3	43.7	–	34.5	8.5	0.0
Hydrogen terminated	12.5	–	1.1	42.4	–	32.7	11.3	0.0
Chlorine terminated	29.4	1.2	5.3	24.4	2.4	22.0	15.2	0.1
Alkene terminated	34.7	3.5	4.2	13.7	9.3	10.8	23.8	0.0
Grubbs primed	26.0	3.0	3.2	19.7	6.8	17.1	23.8	0.5
Carboxyl terminated	52.4	1.5	1.2	14.4	3.6	10.2	16.4	0.3
Hexylamine terminated	61.0	–	0.5	13.2	–	12.0	13.1	0.1
Peptide terminated	65.8	–	0.2	3.2	–	12.9	17.9	0.0

All data are displayed in atomic percentages. The atomic percentages were calculated from XPS spectra obtained following each step in the reaction scheme using Eq. (1). For data displayed in the table, the detector was positioned normal to the sample surface (photoemission angle of 0°). The Ga concentrations were calculated from the Ga 3d spectra. The dash (–) in several of the fields indicates the absence of an element within XPS detection limits.

The photoemission intensity from a uniform adlayer is given by Eq. (6)[54].

$$N_l(\theta) = I_0\Omega_0(E_l)A_0(E_l)D_0\rho_{adlayer}\frac{d\sigma_l}{d\Omega}\Lambda_e^{adlayer}(E_l)\ cos\ \theta\left[1-exp\left(\frac{-t}{\Lambda_e^{adlayer}(E_l)\ cos\ \theta}\right)\right] \quad (6)$$

The ratio of the intensity of the photoemission from the adlayer to the photoemission from the substrate is obtained by dividing Eq. (6) by Eq. (4)[54]. Several simplifications are possible if photoelectrons with similar kinetic energy from the adlayer and substrate are used, such as when using peaks from the same subshell. Simplifying and solving for t gives Eq. (7).

$$t = \Lambda_e^{adlayer}\left(E_{l,s}\right)\ cos\ \theta\ ln\left[\frac{N_l(\theta)\rho_{subst}\Lambda_e^{subst}(E_s)}{N_s(\theta)\rho_{adlayer}\Lambda_e^{adlayer}\left(E_{l,s}\right)}+1\right] \quad (7)$$

The simplifications that resulted in Eq. (7) include canceling the I_0, D_0, $cos\theta$, Ω_o, A_0, and $d\sigma/d\Omega$ terms. With adlayer and substrate photoemission peaks from the same subshell, $\Lambda_e^{adlayer}(E_l)$ and $\Lambda_e^{adlayer}(E_s)$ are nearly equal and were replaced with $\Lambda_e^{adlayer}(E_{l,s})$ which is the attenuation length from the substrate or adlayer through the adlayer. $N_l(\theta)$ and $N_s(\theta)$ are the intensities from the adlayer and substrate, $\rho_{adlayer}$ and ρ_{subst} are the atomic densities of the adlayer and substrate, and $\Lambda_e^{subst}(E_s)$ is the attenuation length of a photoelectron from the substrate through the substrate. Eq. (7) was used to calculate the adlayer thickness in the third data column of Table 6.

4. Results and discussion

4.1. Qualitative XPS study of reaction steps

High resolution XPS spectra were obtained for Cl 2p, Ga $2p_{3/2}$, O 1s, N 1s, C 1s, Ga 3d, Ca 2p, and Mg 2p following each step of the reaction scheme. Each of these spectra was collected at angles of 0°, 45°, and 60° from surface normal.

Figs. 2 and 3 show the Ga 2p and Ga 3d spectra obtained after each reaction step. Of these two spectra, the Ga $2p_{3/2}$ is more surface sensitive since the kinetic energy of the Ga $2p_{3/2}$ photoelectron is ~370 eV while the kinetic energy of the Ga 3d photoelectron is ~1467 eV with the Al Kα radiation. With the Ga $2p_{3/2}$ core electrons having a lesser kinetic energy, the information depth from which photoelectrons can reach an energy analyzer is reduced. The surface sensitivity of Ga $2p_{3/2}$ is apparent when comparing the EAL of the Ga $2p_{3/2}$ and Ga 3d photoelectrons through GaN. EALs of Ga $2p_{3/2}$ and Ga 3d are 0.7 nm and 2.2 nm, respectively [61]. Due to the greater surface sensitivity of Ga $2p_{3/2}$ in comparison to Ga 3d, the similarity of the Ga $2p_{3/2}$ peak positions and shapes of Fig. 2 is especially significant in detecting the formation of gallium oxide at the GaN surface. The Ga $2p_{3/2}$ peak from Ga–N is observed at 1117.1 eV. The absence of an additional peak/shoulder at a higher binding energy indicates negligible oxidation of the surface Ga atoms. The low signal to noise ratio for the peptide-terminated sample is due to the attenuation of the Ga $2p_{3/2}$ signal by the thick peptide layer.

Hydrogen or chlorine termination passivates semiconductor surfaces and inhibits the surfaces from reacting with the atmosphere during sample preparation before functionalizing the surface with organic molecules [28]. As shown in Fig. 4, the intensity of the Cl 2p peaks greatly increased with the binding of chlorine to the GaN surface. Additionally, the presence of a second Cl 2p doublet at a higher binding energy in the spectra corresponding to the chlorine-terminated sample may indicate Cl–Ga bonds on the surface. However, the presence of this second doublet has not consistently appeared in previous experimental runs. The presence of chlorine on the sample surface throughout the reaction scheme is likely due to the presence of chloride ions in the solvents used in the reaction steps. This is especially true following the alkene-termination of the GaN surface using allylmagnesium chloride where a form of chlorine

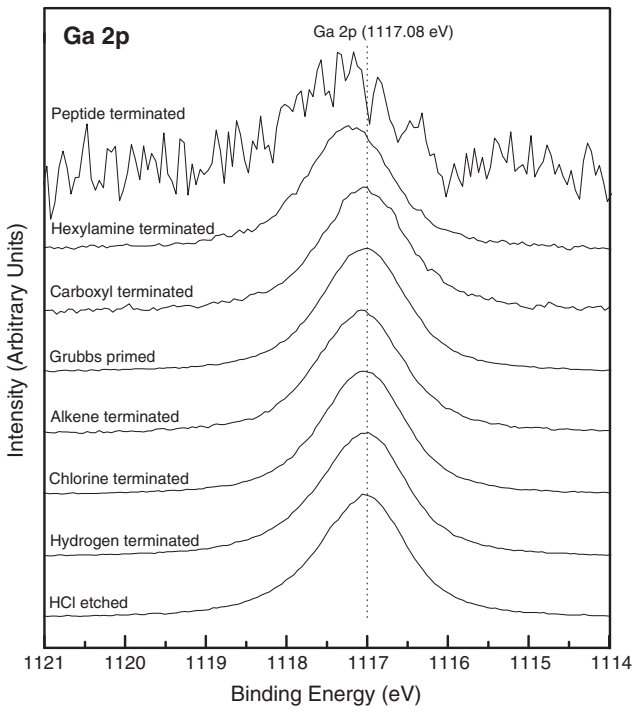

Fig. 2. Ga $2p_{3/2}$ high resolution XPS spectra of the GaN surfaces following each step of the reaction scheme. Each peak was normalized for ease of comparison of peak positions and widths. XPS spectra shown were collected in normal direction to the sample surface. The dotted line indicates the mean binding energy of the displayed peaks.

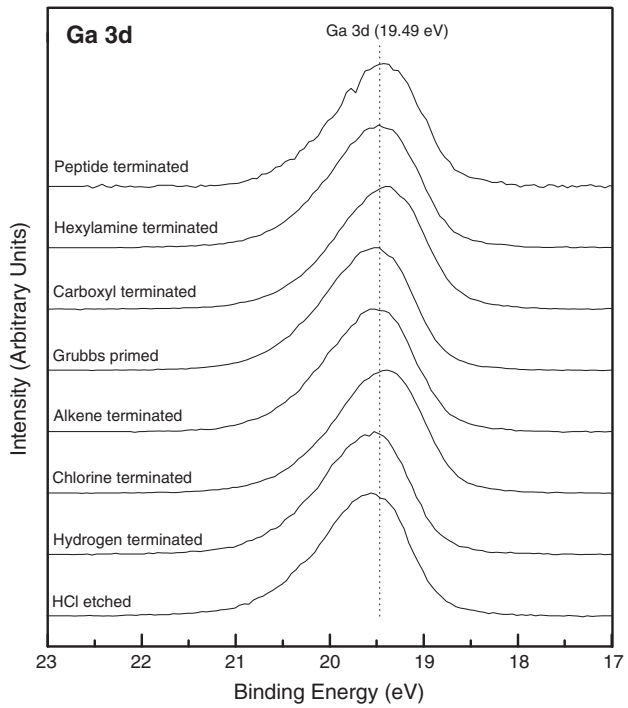

Fig. 3. Ga 3d high resolution XPS spectra of the GaN surfaces following each step of the reaction scheme. Each peak was normalized for ease of comparison of peak positions and widths. XPS spectra shown were collected in normal direction to the sample surface. The dotted line indicates the mean binding energy of the displayed peaks.

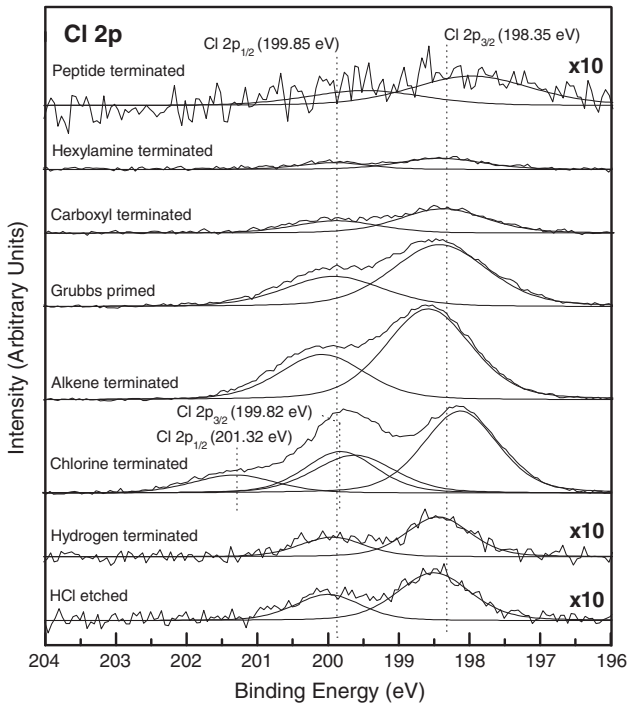

Fig. 4. Cl 2p high resolution XPS spectra of the GaN surfaces following each step of the reaction scheme. The intensities of the HCl etched, hydrogen plasma treated, and peptide-terminated surfaces were multiplied by a factor of 10 for clarity. XPS spectra shown were collected in normal direction to the sample surface. The dotted lines indicate the mean binding energies of the displayed peaks.

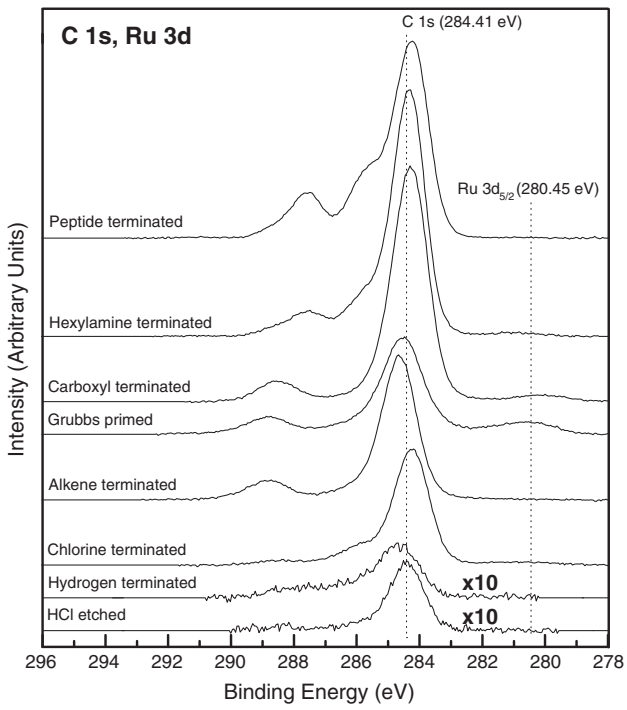

Fig. 5. C 1s and Ru 3d high resolution XPS spectra of the GaN surfaces following each step of the reaction scheme. The intensities of the HCl etched and hydrogen terminated surfaces were multiplied by a factor of 10 for clarity. XPS spectra shown were collected in normal direction to the sample surface. The dotted lines indicate the mean binding energies of the displayed peaks. Note that the Ru $3d_{5/2}$ peak is only present on the Grubbs primed and carboxyl-terminated samples.

remained on the surface despite an extensive washing procedure with THF.

Since the GaN samples were exposed to ambient air following each step of the reaction scheme, adsorbed hydrocarbons were likely present on the surface. The adsorbed carbon species are readily apparent in the C 1s spectra shown in Fig. 5 following HCl etch, hydrogen termination, and chlorine termination. In the remaining spectra of Fig. 5, C 1s peaks are expected due to the intentional functionalization of the surface with carbon containing molecules, but residual hydrocarbons likely contribute as well.

Due to the ruthenium atom within the Grubbs catalyst, two C 1s spectra in Fig. 5 contain the Ru 3d contributions. In the spectrum corresponding to the sample primed with Grubbs first generation catalyst, the presence of the Ru $3d_{5/2}$ peak indicates that the catalyst bound to the GaN surface. This peak was reduced in intensity, but lingered, following the carboxyl termination of the surface through olefin cross-metathesis. The continued presence of this peak may indicate that a portion of the catalyst was still bound to the surface due to the cross-metathesis reaction not reaching completion. Alternatively, the catalyst may have remained physisorbed on the surface despite extensive washing in dichloromethane. The contributions of the Ru 3d peaks to the C 1s spectra are displayed in detail in Fig. 6. The peak fitting constraints for the Ru 3d peaks include setting the ratio of the peak areas of the Ru $3d_{5/2}$ to Ru $3d_{3/2}$ peaks as 3:2 with a spin-orbital doublet separation defined as 4.15 eV.

The spectra of Fig. 6 were fitted with peak components based on the expected molecular structures on the surface that are displayed in Scheme 1. All curve fitting was performed using CasaXPS software version 2.3.12 (www.casaxps.com) and the ratios stated in this section. In the carboxyl-terminated spectrum that was acquired following the binding of 6-heptenoic acid, the ratio of the peak areas for the carboxyl carbon peak to the alkane peak was 1:7 to account for the carbon chain of seven carbon atoms with a terminal carboxyl group. For the spectrum in Fig. 6 following the binding of hexylamine

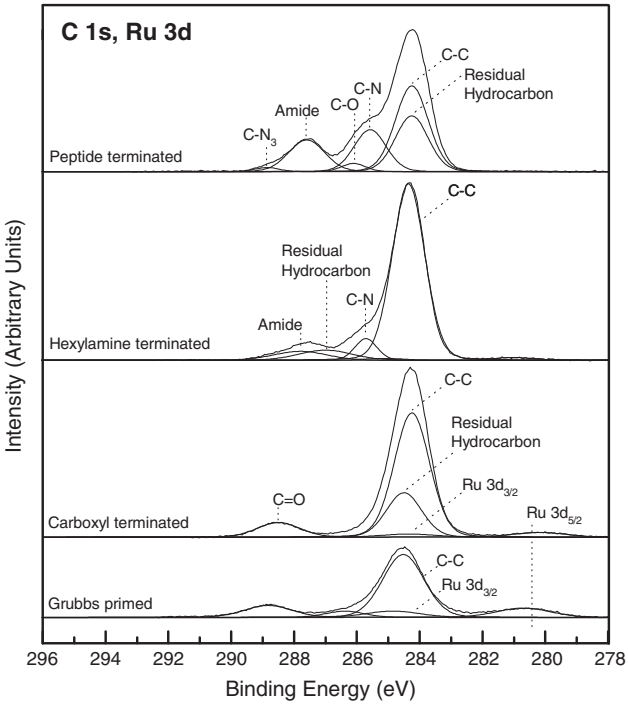

Fig. 6. C 1s and Ru 3d high resolution XPS spectra of the GaN surfaces following the priming of the surface with Grubbs first generation catalyst, terminating the surface with a carboxyl group via olefin cross-metathesis, and binding hexylamine or a peptide to the surface with a condensation reaction. These spectra are the same as the uppermost four spectra of Fig. 5 with the peak fitting components displayed. XPS spectra shown were collected in normal direction to the sample surface.

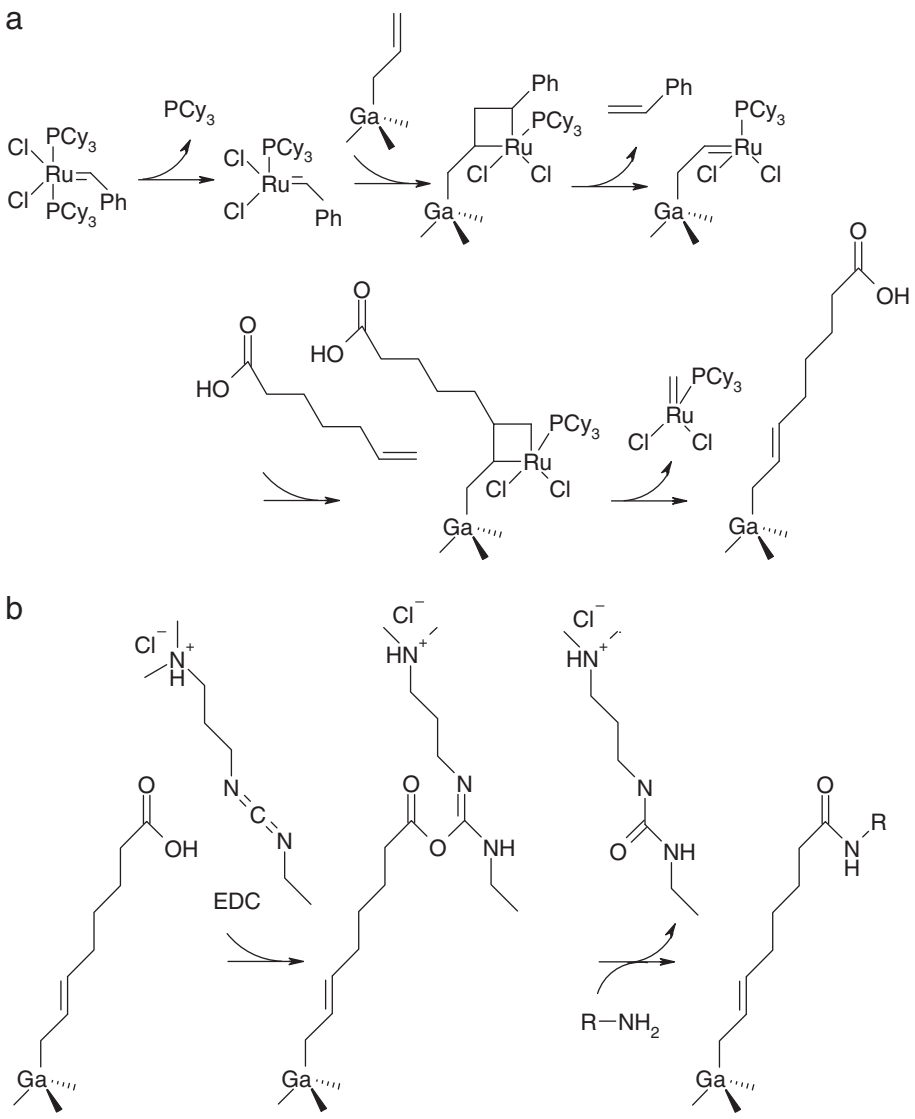

Scheme 1. a. Olefin metathesis reaction used to bind 6-heptenoic acid to an alkene-terminated GaN surface. The reaction mechanism is based on Sanford et al. [53] b. EDC catalyzed amide bond formation at the GaN surface. R represents $(CH_2)_5CH_3$ or the peptide NYQWVPYQGRVPYPRPGTC.

to the terminal carboxyl group, the ratio of the C–C, C–N, and amide C peaks was 12:1:1. For the peptide-terminated C 1s spectrum, the ratio of the C–C, C–N, C–O, amide, and $C-N_3$ peaks was 57:27:4:23:2. This ratio accounted for the peptide structure and the eight carbon chain shown in the final step of Scheme 1 connecting the R group to the GaN surface. In the carboxyl, hexylamine, and peptide terminated sample spectra, the residual hydrocarbon peaks accounted for the remaining area under the C 1s spectrum and are attributed to contamination.

With the overlap of the Ga Auger and N 1s peaks with an Al Kα radiation source, peak fitting was necessary to determine the contributions of the N 1s and Ga LMM peaks to the spectra in Fig. 7. The ratio of areas of the Ga LMM 1, Ga LMM 2, and Ga LMM 3 peaks was set to 0.252:1:0.102, which was determined through a number of samples. The GaN, amine, and amide peaks were left to fill the remaining area of the spectra.

Evidence of the amide bond forming when hexylamine or the peptide bound to the terminal surface carboxyl group is evident in the two uppermost spectra of Fig. 7. According to the literature, the peak at a binding energy of ~400 eV indicates the presence of an amide or an amine group [62]. In Fig. 7, the peak at 399.5 eV is not present in any N 1s spectra from steps earlier in the reaction scheme. When hexylamine binds, only one nitrogen atom on the molecule is available to contribute to the amide bond. For this reason, the peak at 399.5 eV is due solely to the amide bond. The peak at 399.5 eV of the peptide terminated surface is due to amide bonds connecting amino acid residues and the W, R, N, and Q residues that contain additional nitrogen atoms in their side chains. Since the amine terminus of the peptide and the W and R residues all provide amine groups to bind to the carboxyl group on the GaN surface, the orientation of peptide binding to the surface was not predictable.

4.2. Surface element composition

As discussed in the Materials and methods section, the surface element composition was calculated from the XPS data following each step of the reaction scheme using Eq. (1). This method assumes a homogeneous distribution of elements in the near surface region. The surface element compositions are reported in Table 1.

The presence of adsorbed carbon on the GaN surface from exposure to ambient air is apparent in Table 1. The HCl etched, hydrogen plasma treated, and the chlorinated samples all had adsorbed carbon species. This is typical for a sample transferred through air for XPS analysis. Through subsequent reaction steps, the

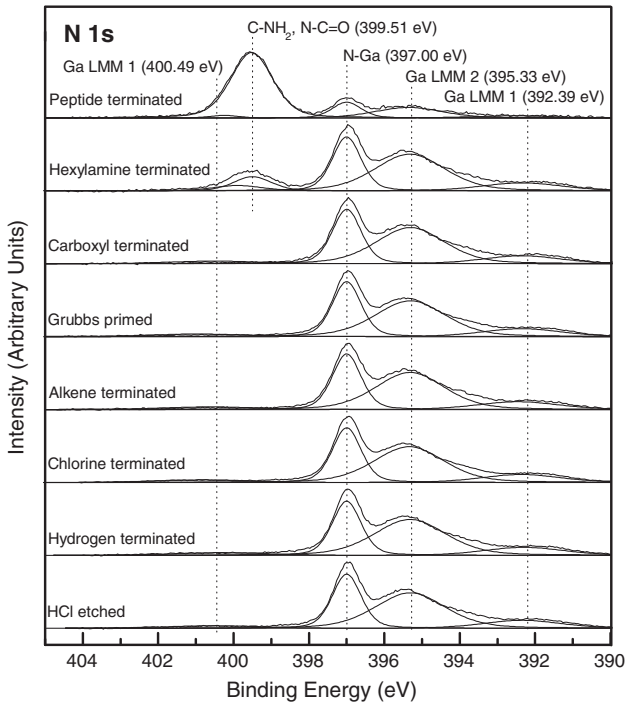

Fig. 7. N 1s core level and Ga X-ray excited Auger spectra of the GaN (0001) surfaces following each step of the reaction scheme. Each peak was normalized for ease of comparison of peak positions and widths. XPS spectra shown were collected in normal direction to the sample surface. The dotted lines indicate the mean binding energies of the displayed peaks. Note that peaks corresponding to amide and amine bonds appear on the hexylamine and peptide samples only.

surface carbon concentration increased as expected. The binding of an alkene functional group to the surface led to a further increase in carbon concentration. Additional increases resulted as the hydrocarbon molecule on the surface increased in length through the carboxyl termination, hexylamine termination, and peptide termination steps.

In addition to the carbon contamination from atmospheric exposure, various other surface contaminants were present on the surface in low levels. The presence of Ca, Mg, and Cl in the solvents used in the reaction steps may explain the presence of these species (Table 1). Additionally, the formation of carbonates with calcium and magnesium on the surface may account for at least a portion of the surface oxygen. Despite the surface contamination throughout the reaction scheme, the chlorine concentration was greatest for the chlorine-terminated GaN sample as expected.

As mentioned in the previous subsection, the presence of ruthenium on the Grubbs primed surface indicates the binding of the catalyst to the surface. Table 1 shows no ruthenium on the GaN surface prior to the Grubbs catalyst priming step and 0.5 at.% ruthenium following the catalyst priming. The decrease in ruthenium atomic percent from 0.5 at.% to 0.3 at.% in the carboxyl termination step indicates that a portion of the catalyst was replaced during the olefin cross-metathesis reaction that bound 6-heptenoic acid to the surface. The presence of ruthenium on the chlorine-terminated sample was likely due to contamination in the glassware since the Ru 3d peak was not present on the chlorine-terminated samples in previous experimental runs [51].

Gallium and nitrogen concentrations are shown in Table 1. The nitrogen column of Table 1 includes contributions from both GaN substrate and adlayer nitrogen atoms. The general trend of the gallium and nitrogen concentrations is to decrease with each step of the reaction which is an effect of increased attenuation as the length of the surface molecules increases. The exception to this is the increase in nitrogen concentration when hexylamine or the peptide was bound to the carboxyl-terminated sample. This nitrogen increase indicates the addition of the nitrogen atoms in hexylamine and the peptide.

Table 2
GaN substrate composition in the near surface region.

	Ga, %	N, %
HCl etched	55.9	44.1
Hydrogen terminated	56.5	43.5
Chlorine terminated	52.6	47.4
Alkene terminated	55.9	44.1
Grubbs primed	53.6	46.4
Carboxyl terminated	58.6	41.4
Hexylamine terminated	59.8	40.2
Peptide terminated	63.9	36.1

Data is based on the Ga 3d spectra and the GaN component of the N 1s spectra collected normal to the sample surface. Atomic percentages were calculated using Eq. (1).

The substrate composition in the near surface region is shown in Table 2. Gallium and nitrogen concentrations were normalized to 100% and therefore the Ga 3d peak and only the N-Ga component of the N 1s spectra were used to calculate the percentages. According to Table 2, the composition of the GaN substrate consisted nearly equally of gallium and nitrogen following the HCl etch, hydrogen termination, and chlorine termination steps. However, the percentage of nitrogen decreased with subsequent steps in the reaction scheme. This is a result of the failure of the homogeneous distribution assumption used in Eq. (1). Each step in the reaction scheme resulted in an increase in adlayer thickness. Since N 1s has a lower kinetic energy than Ga 3d, a thicker adlayer leads to higher attenuation of the N 1s photoelectrons in comparison to the Ga 3d photoelectrons. Since the reaction steps following surface chlorination are unlikely to change the substrate composition at the interface with the adlayer, the nearly 1:1 gallium to nitrogen ratio of the substrate early in the scheme likely persisted throughout the entire scheme despite the results of Table 2.

Table 3 shows the experimental and theoretical values of the ratios of carbon to oxygen and carbon to nitrogen. Theoretical ratios are based on the number of carbon, oxygen, and nitrogen atoms that compose the molecule bound to the surface as displayed in Scheme 1. All of the experimental carbon to oxygen ratios are less than the theoretical values. The presence of a larger amount of surface oxygen than expected will decrease the experimental carbon to oxygen ratio. Calcium carbonate and magnesium carbonate are potential sources of unexpected surface oxygen. In contrast to the differing experimental and theoretical carbon to oxygen ratios, the experimental and theoretical carbon to nitrogen ratios are quite close. This verifies the validity of the C 1s and N 1s peak fitting procedure described earlier.

4.3. Surface coverage

Eq. (2) was used to calculate the coverage of the GaN (0001) surface following each step of the reaction scheme. We note that contamination can significantly alter the coverage and thickness calculations and has been previously discussed by van der Marel et al. [63]. The results are displayed in Table 4 as monolayers (ML) of *atomic*

Table 3
Experimental and theoretical atomic ratios.

	Experimental C/O	Theoretical C/O	Experimental C/N	Theoretical C/N
Carboxyl terminated	2.1	4	–	–
Hexylamine terminated	4.3	14	14.5	14
Peptide terminated	2.6	4.2	4.1	3.8

All experimentally derived ratios are the mean of the ratios calculated from data collected at 0°, 45°, and 60° to surface normal. The residual hydrocarbon components of the C 1s spectra were excluded from the calculations. The ratios were derived from data obtained with Eq. (1).

Table 4
Atomic Surface Coverages.

	Cl 1s, ML		Ru 3d, ML		Carbonyl peak of C 1s, ML		Amide peak of N 1s, ML	
	Ga 3d	N 1s	Ga 3d	N 1s	Ga 3d	N 1s	Ga 3d	N 1s
HCl etched	0.12	0.14	0.00	0.00	0.06	0.07	0.00	0.00
Hydrogen terminated	0.10	0.12	0.00	0.00	0.15	0.19	0.00	0.00
Chlorine terminated	0.70	0.76	0.02	0.02	0.15	0.16	0.00	0.00
Alkene terminated	1.37	1.58	0.00	0.00	1.47	1.70	0.00	0.00
Grubbs primed	0.69	0.80	0.13	0.15	0.86	0.99	0.00	0.00
Carboxyl terminated	0.36	0.55	0.08	0.12	1.15	1.71	0.00	0.00
Hexylamine terminated	0.18	0.25	0.05	0.06	1.93	2.70	1.83	2.58
Peptide terminated	0.26	0.48	0.00	0.00	16.56	29.97	14.55	26.28

Atomic coverage values were calculated using Eq. (2) for XPS data collected at photoemission angles of 0°, 45°, and 60°. The mean value of the three calculations is displayed in the table in monolayers (ML). The uppermost column headings indicate the XPS peak used for $N_l(\theta)$ in Eq. (2), and the secondary column headings indicate whether the Ga 3d peak or N 1s peak was used for $N_s(\theta)$ in Eq. (2).

species on the GaN (0001) surface. In Table 4 a monolayer is the ratio of the number of adlayer atomic species to the number of substrate surface atoms. The intensities of Cl 1s, Ru 3d, the carbonyl component of C 1s, and the amide component of N 1s were used for $N_l(\theta)$, the adlayer signal intensity. The intensity of Ga 3d was used for $N_s(\theta)$, the substrate signal intensity. Since Ga 3d photoelectrons have a greater kinetic energy than the Ga $2p_{3/2}$ photoelectrons, the Ga 3d photoelectrons will experience less attenuation when passing through the adlayer. The result is a calculation that more closely follows the non-attenuation approximation. For comparison, Table 4 also displays coverage when the GaN component of the N 1s spectra was used for $N_s(\theta)$ instead of the Ga 3d spectra. The Ga 3d or N 1s average effective electron attenuation lengths were used for λ_e^{subst} and were generated with the NIST Electron Effective-Attenuation-Length Database [61]. The surface coverage was calculated for the XPS data collected at 0°, 45°, and 60° from surface normal. The means of these three values are reported in Table 4.

As shown in Table 4, the chlorine coverage greatly increased from the etching step to the chlorine termination step. This is as expected since the goal of the chlorination step is to passivate the GaN surface by binding chlorine atoms to the surface gallium atoms. However, the chlorine coverage further increased following the alkene-termination step. This is due to the chlorine in the allylmagnesium chloride that persisted on the GaN surface despite extensive washing in THF. The chlorine coverage decreased in subsequent steps of the reaction scheme.

The coverage of the Grubbs first generation catalyst is displayed in the Ru 3d column of Table 4. With only a single ruthenium atom in each catalyst molecule, the ruthenium coverage is equivalent to the Grubbs catalyst molecular coverage. When the GaN surface was primed with the Grubbs catalyst, the coverage of the catalyst on the surface was 0.13 monolayers based on the Ga 3d substrate peak. The coverage dropped in the next step as the Grubbs catalyst was replaced by the binding of 6-heptenoic acid through the olefin cross-metathesis reaction.

The Carbonyl Peak column of Table 4 displays the coverage of the GaN surface with carbonyl carbon atomic species. To specifically calculate the coverage of carbonyl carbons, the peaks in the C 1s spectra near 288 to 289 eV were used for $N_l(\theta)$ in Eq. (2). Table 4 shows carbonyl contamination from the HCl etching step to the Grubbs priming step since the functionalization of these surfaces in these steps did not intentionally bind carbonyl groups. The carboxyl terminated and hexylamine terminated samples were both functionalized with surface molecules containing a single carbonyl carbon per molecule. The peptide terminated surface was functionalized with a peptide containing 23 carbonyl carbons per molecule. The increase in carbonyl atomic coverage of the carboxyl terminated, hexylamine terminated, and peptide terminated surface in Table 4 reflects the binding of the respective molecular structures. However, an undetermined portion of these coverages were due to the carbonyl surface contamination. This contamination by carbonyl species resulted in an overestimation of the coverage based on the carbonyl component of the C 1s spectra.

Coverage of the hexylamine and peptide terminated surfaces was also calculated based on the amide peak of the N 1s spectra for $N_l(\theta)$ of Eq. (2). These results are shown in the Amide peak column of Table 4. With only a single amide bond per molecule, the amide coverage of the hexylamine terminated surface was the same as the molecular coverage. However, the peptide terminated surface had multiple amide and amine species per molecule. Since only a single peak was defined for the amide and amine groups on the peptide terminated N 1s spectra, a fraction of the peak intensity was needed for the amide nitrogen coverage calculation. For the peptide terminated surface, the intensity of the amide/amine peak was multiplied by 23/30 to account for the ratio of amide nitrogen atoms to all nitrogen atoms in the molecule. The resulting peak intensity was used for $N_l(\theta)$ of Eq. (2). As shown in the Amide Peak column of Table 4, none of the GaN surfaces prior to functionalization with hexylamine or the peptide had amide surface species. The amide coverage of the hexylamine and peptide terminated surfaces are due solely to the surface functionalization without components from contamination.

For Table 5 the values of Table 4 were divided by the number of carbonyl carbon atoms or amide nitrogen atoms in the surface bound molecule, as shown in Scheme 1, to give the *molecular* coverage for the carboxyl, hexylamine, and peptide terminated GaN wafers. These coverages were calculated from Eq. (2) which assumes a non-attenuating adlayer on the substrate. This non-attenuation approximation probably fails with adlayers of increasing thickness. The coverages surpassing 1 monolayer in Table 5 may have resulted from the attenuation of the substrate photoelectrons by the increasing thickness of the adlayer. When hexylamine bound to the terminal carboxyl group, the resulting molecule was 14 carbons long, and the non-attenuating approximation is incorrect with a molecule of this length bound to the GaN surface. The approximation is probably even worse with the peptide terminated surface. The result of substrate photoelectron attenuation is a lower value for $N_s(\theta)$ and a coverage result that is artificially high. The molecular coverages based on the N 1s substrate signal are higher than those based on Ga 3d due to the lower kinetic energy of the N 1s photoelectron that suffers greater attenuation through the adlayer.

With the overestimated coverages in Table 5 as an upper limit of the actual coverage, the lower limit is likely near 0.13 monolayers since this is the coverage of Grubbs catalyst following the catalyst priming of the GaN surface. In previous work done in this laboratory, the molecular coverage following olefin cross-metathesis was similar to that of the Grubbs catalyst coverage [51].

4.4. Adlayer thickness

Table 6 provides a comparison of adlayer calculation results by using Eqs. (5) and (7). The first two data columns of Table 6 were

Table 5
Molecular surface coverages.

	Carbonyl peak of C 1s, ML		Amide peak of N 1s, ML	
	Ga 3d	N 1s	Ga 3d	N 1s
Carboxyl terminated	1.15	1.71	0.00	0.00
Hexylamine terminated	1.93	2.70	1.83	2.58
Peptide terminated	0.72	1.30	0.63	1.14

The coverage values were derived from the values of Table 4 divided by the number of the particular atomic species in the molecule as shown in Scheme 1. (ML = monolayer).

Table 6
Adlayer thicknesses.

	Calculated with Eq. (5)		Calculated with Eq. (7)	Theoretical thickness
	Ga 3d	N 1s	Amide and GaN peaks of N 1s	
Carboxyl terminated	2.9 nm	3.3 nm	–	0.996 nm
Hexylamine terminated	4.9 nm	4.4 nm	5.1 nm	1.731 nm
Peptide terminated	5.3 nm	4.0 nm	7.6 nm	4.596 nm

The thicknesses displayed in the first and second data columns were calculated with Eq. (5) and the graphic method described in the Calculations section. The thicknesses displayed in the third data column are the mean thicknesses calculated for XPS data collected at 0°, 45°, and 60° to surface normal.

calculated using the XPS spectra of an argon-sputtered GaN surface as the bare substrate sample. The intensities of the Ga 3d or N 1s peaks of this bare substrate were used for $N_s^0(\theta)$ of Eq. (5). The Ga 3d peak or the GaN component of the N 1s peak of the carboxyl, hexylamine, and peptide terminated GaN wafers was used for $N_s(\theta)$. Errors in the thickness calculations may have resulted from using a different sample for the functionalized and bare surfaces due to slight differences in sample positioning during XPS acquisition. Also, Ar sputtering does not exactly produce a bare GaN surface due to preferential sputtering. The attenuation lengths of the different adlayers, $\Lambda_e^{adlayer}(E_s)$, were calculated by a procedure described by Cumpson to estimate the inelastic mean free paths of organic materials [64].

Eq. (7) was used to calculate the adlayer thicknesses for the third data column of Table 6. $\Lambda_e^{adlayer}(E_{l,s})$ was replaced with the inelastic mean free path through the adlayer as estimated with Cumpson's method [64]. The amide component of the N 1s spectra was used for $N_l(\theta)$, $\Lambda_e^{subst}(E_s)$ was estimated by the NIST Electron Effective-Attenuation-Length Database [61], and the GaN peak of the N 1s spectra was used for $N_s(\theta)$. ρ_{subst} was calculated as 4.423×10^{22} cm^{-3} by using the density and molar mass of GaN. $\rho_{adlayer}$ was estimated as 2.694×10^{21} cm^{-3} for the hexylamine terminated surface by estimating the adlayer molar volume at room temperature using a method described by Bicerano [65]. $\rho_{adlayer}$ was estimated as 1.087×10^{22} cm^{-3} for the peptide terminated surface by using an estimated peptide volume of 2761 Å^3 derived by the Peptide Property Calculator [66].

The thickness values calculated from Eq. (7) are likely more accurate than those calculated from Eq. (5) since the Eq. (7) results were each calculated from the data of a single sample. The theoretical carboxyl and hexylamine termination thicknesses were acquired from the software package ACD/3D version 4.52 (www.acdlabs.com), and the theoretical peptide termination thickness was acquired from Chem3D Pro version 12.0 by CambridgeSoft (www.cambridgesoft.com). All experimental adlayer thicknesses are greater than the theoretical values. This indicates that more than a monolayer was present on the surfaces.

5. Conclusion

This work has demonstrated the covalent binding of two organic molecules, hexylamine and a peptide, to the GaN (0001) surface. Greater than one monolayer of coverage was achieved. By using a reaction scheme based on olefin cross-metathesis, this reaction is easily tailored to binding a wide variety of organic molecules to the GaN surface. Changing the functional groups on the alkene-terminated molecule that binds to the surface during the olefin cross-metathesis will allow changes to the overall surface functionalization. In addition to the versatility of this route, the method demonstrated in this work is able to functionalize the GaN surface directly and does not rely on functionalizing layers grown on the GaN surface. For field effect transistor biosensing applications, direct GaN surface functionalization will result in a gate surface that is closer to the channel and will provide greater sensitivity for analyte detection.

Acknowledgments

This work was supported by NSF under CMMI-0856391. We acknowledge MSTP (NIH GM077229) for financial support. Instructional materials used to engage undergraduate students in this research were made possible by National Science Foundation Undergraduate Research Center award (CHE-0418902) that supports the Center for Authentic Science Practice in Education (CASPiE). We thank members of the Panitch Lab for help with reagents and useful discussions.

Appendix A. Supplementary data

Supplementary data to this article can be found online at doi:10.1016/j.susc.2011.05.015.

References

[1] A.P. Zhang, F. Ren, T.J. Anderson, C.R. Abernathy, R.K. Singh, P.H. Holloway, S.J. Pearton, D. Palmer, Crit. Rev. Solid State Mater. Sci. 27 (2002) 1.
[2] A.P. Zhang, G. Dang, F. Ren, J. Han, C. Monier, A.G. Baca, X.A. Cao, H. Cho, C.R. Abernathy, S.J. Pearton, Solid-State Electron. 46 (2002) 933.
[3] X.A. Cao, S.J. Pearton, F. Ren, Crit. Rev. Solid State Mater. Sci. 25 (2000) 279.
[4] N. Chaniotakis, N. Sofikiti, Anal. Chim. Acta 615 (2008) 1.
[5] T.H. Young, C.R. Chen, Biomaterials 27 (2006) 3361.
[6] S.J. Pearton, B.S. Kang, S.K. Kim, F. Ren, B.P. Gila, C.R. Abernathy, J.S. Lin, S.N.G. Chu, J. Phys. Condens. 16 (2004) R961.
[7] S.J. Pearton, F. Ren, Adv. Mater. (Weinheim, Ger.) 12 (2000) 1571.
[8] B.S. Kang, H.T. Wang, F. Ren, S.J. Pearton, J. Appl. Phys. 104 (2008) 03110.
[9] B.S. Kang, F. Ren, M.C. Kang, C. Lofton, W.H. Tan, S.J. Pearton, A. Dabiran, A. Osinsky, P.P. Chow, Appl. Phys. Lett. 86 (2005) 173502.
[10] B.S. Kang, H.T. Wang, F. Ren, S.J. Pearton, T.E. Morey, D.M. Dennis, J.W. Johnson, P. Rajagopal, J.C. Roberts, E.L. Piner, K.J. Linthicum, Appl. Phys. Lett. 91 (2007) 252103.
[11] B.H. Chu, B.S. Kang, F. Ren, C.Y. Chang, Y.L. Wang, S.J. Pearton, A.V. Glushakov, D.M. Dennis, J.W. Johnson, P. Rajagopal, J.C. Roberts, E.L. Piner, K.J. Linthicum, Appl. Phys. Lett. 93 (2008) 042114.
[12] B.S. Kang, F. Ren, L. Wang, C. Lofton, W.H.W. Tan, S.J. Pearton, A. Dabiran, A. Osinsky, P.P. Chow, Appl. Phys. Lett. 87 (2005) 023508.
[13] B.S. Kang, H.T. Wang, T.P. Lele, Y. Tseng, F. Ren, S.J. Pearton, J.W. Johnson, P. Rajagopal, J.C. Roberts, E.L. Piner, K.J. Linthicum, Appl. Phys. Lett. 91 (2007) 112106.
[14] H.T. Wang, B.S. Kang, F. Ren, S.J. Pearton, J.W. Johnson, P. Rajagopal, J.C. Roberts, E.L. Piner, K.J. Linthicum, Appl. Phys. Lett. 91 (2007) 222101.
[15] K.H. Chen, B.S. Kang, H.T. Wang, T.P. Lele, F. Ren, Y.L. Wang, C.Y. Chang, S.J. Pearton, D.M. Dennis, J.W. Johnson, P. Rajagopal, J.C. Roberts, E.L. Piner, K.J. Linthicum, Appl. Phys. Lett. 92 (2008) 192103.
[16] B.H. Chu, C.Y. Chang, K. Kroll, N. Denslow, Y.L. Wang, S.J. Pearton, A.M. Dabiran, A.M. Wowchak, B. Cui, P.P. Chow, F. Ren, Appl. Phys. Lett. 96 (2010) 013701.
[17] S. Gupta, M. Elias, X.J. Wen, J. Shapiro, L. Brillson, W. Lu, S.C. Lee, Biosens. Bioelectron. 24 (2008) 505.
[18] Y.L. Wang, B.H. Chu, K.H. Chen, C.Y. Chang, T.P. Lele, G. Papadi, J.K. Coleman, B.J. Sheppard, C.F. Dungen, S.J. Pearton, J.W. Johnson, P. Rajagopal, J.C. Roberts, E.L. Piner, K.J. Linthicum, F. Ren, Appl. Phys. Lett. 94 (2009) 243901.
[19] Y.L. Wang, B.H. Chu, K.H. Chen, C.Y. Chang, T.P. Lele, Y. Tseng, S.J. Pearton, J. Ramage, D. Hooten, A. Dabiran, P.P. Chow, F. Ren, Appl. Phys. Lett. 93 (2008) 262101.
[20] B.S. Kang, S.J. Pearton, J.J. Chen, F. Ren, J.W. Johnson, R.J. Therrien, P. Rajagopal, J.C. Roberts, E.L. Piner, K.J. Linthicum, Appl. Phys. Lett. 89 (2006) 122102.
[21] G. Steinhoff, B. Baur, G. Wrobel, S. Ingebrandt, A. Offenhausser, A. Dadgar, A. Krost, M. Stutzmann, M. Eickhoff, Appl. Phys. Lett. 86 (2005) 033901.
[22] J.J. Yu, S.K. Jha, L.D. Xiao, Q.J. Liu, P. Wang, C. Surya, M. Yang, Biosens. Bioelectron. 23 (2007) 513.
[23] S.J. Pearton, D.P. Norton, F. Ren, Small 3 (2007) 1144.
[24] A. Ganguly, C.P. Chen, Y.T. Lai, C.C. Kuo, C.W. Hsu, K.H. Chen, L.C. Chen, J. Mater. Chem. 19 (2009) 928.
[25] C.P. Chen, A. Ganguly, C.H. Wang, C.W. Hsu, S. Chattopadhyay, Y.K. Hsu, Y.C. Chang, K.H. Chen, L.C. Chen, Anal. Chem. 81 (2009) 36.
[26] B.N. Park, J.J. Uhlrich, T.F. Kuech, P.G. Evans, J. Appl. Phys. 106 (2009) 5.
[27] T.L. Lasseter, B.H. Clare, N.L. Abbott, R.J. Hamers, J. Am. Chem. Soc. 126 (2004) 10220.
[28] R.J. Hamers, Annu. Rev. Anal. Chem. 1 (2008) 707.
[29] V.M. Bermudez, Appl. Surf. Sci. 119 (1997) 147.
[30] V.M. Bermudez, Surf. Sci. 417 (1998) 30.
[31] V.M. Bermudez, Chem. Phys. Lett. 317 (2000) 290.
[32] V.M. Bermudez, Surf. Sci. 519 (2002) 173.
[33] V.M. Bermudez, Surf. Sci. 499 (2002) 109.

[34] V.M. Bermudez, Surf. Sci. 499 (2002) 124.
[35] V.M. Bermudez, Langmuir 19 (2003) 6813.
[36] V.M. Bermudez, J.P. Long, Surf. Sci. 450 (2000) 98.
[37] R. Stine, B.S. Simpkins, S.P. Mulvaney, L.J. Whitman, C.R. Tamanaha, Appl. Surf. Sci. 256 (2010) 4171.
[38] L.C. Grabow, J.J. Uhlrich, T.F. Kuech, M. Mavrikakis, Surf. Sci. 603 (2009) 387.
[39] H. Kim, P.E. Colavita, K.M. Metz, B.M. Nichols, B. Sun, J. Uhlrich, X.Y. Wang, T.F. Kuech, R.J. Hamers, Langmuir 22 (2006) 8121.
[40] H. Kim, P.E. Colavita, P. Paoprasert, P. Gopalan, T.F. Kuech, R.J. Hamers, Surf. Sci. 602 (2008) 2382.
[41] T. Ito, S.M. Forman, C. Cao, F. Li, C.R. Eddy, M.A. Mastro, R.T. Holm, R.L. Henry, K.L. Hohn, J.H. Edgar, Langmuir 24 (2008) 6630.
[42] A. Brik, Adv. Synth. Catal. 350 (2008) 1661.
[43] H.E. Blackwell, D.J. O'Leary, A.K. Chatterjee, R.A. Washenfelder, D.A. Bussmann, R.H. Grubbs, J. Am. Chem. Soc. 122 (2000) 58.
[44] P. Schwab, R.H. Grubbs, J.W. Ziller, J. Am. Chem. Soc. 118 (1996) 100.
[45] M.B. Runge, M.T. Mwangi, N.B. Bowden, J. Organomet. Chem. 691 (2006) 5278.
[46] M.T. Mwangi, M.B. Runge, N.B. Bowden, J. Am. Chem. Soc. 128 (2006) 14434.
[47] L. Yang, Y.Y. Lua, M. Tan, O.A. Scherman, R.H. Grubbs, J.N. Harb, R.C. Davis, M.R. Linford, Chem. Mater. 19 (2007) 1671.
[48] S. Dutta, M. Perring, S. Barrett, M. Mitchell, P.J.A. Kenis, N.B. Bowden, Langmuir 22 (2006) 2146.
[49] K.E. Plass, X.L. Liu, B.S. Brunschwig, N.S. Lewis, Chem. Mater. 20 (2008) 2228.
[50] A. Juang, O.A. Scherman, R.H. Grubbs, N.S. Lewis, Langmuir 17 (2001) 1321.
[51] M.S. Makowski, D.Y. Zemlyanov, A. Ivanisevic, Appl. Surf. Sci. 257 (2011) 4625.
[52] J. Mukherjee, S. Peczonczyk, S. Maldonado, Langmuir 26 (2010) 10890.
[53] M.S. Sanford, J.A. Love, R.H. Grubbs, J. Am. Chem. Soc. 123 (2001) 6543.
[54] C.S. Fadley, Basic Concepts of X-ray Photoelectron Spectroscopy, Electron Spectroscopy: Theory, Techniques, and Applications, Academic Press, 1978.
[55] H.P. Wampler, D.Y. Zemlyanov, K. Lee, D.B. Janes, A. Ivanisevic, Langmuir 24 (2008) 3164.
[56] S.S. Jedlicka, J.L. Rickus, D. Zemlyanov, J. Phys. Chem. C 114 (2010) 342.
[57] J.W.J. Slavin, U. Jarori, D. Zemlyanov, A. Ivanisevic, J. Electron. Spectrosc. Relat. Phenom. 172 (2009) 47.
[58] J.W.J. Slavin, D. Zemlyanov, A. Ivanisevic, Surf. Sci. 603 (2009) 907.
[59] R. Flores-Perez, D.Y. Zemlyanov, A. Ivanisevic, J. Phys. Chem. C 112 (2008) 2147.
[60] K.C. Popat, S. Sharma, T.A. Desai, J. Phys. Chem. B 108 (2004) 5185.
[61] NIST Electron Effective-Attenuation-Length Database, SRD-82, version 1.1, National Institute of Standards and Technology, Gaitherburg, MD 20899, USA, 2003.
[62] Z. Xu, P. Hu, S. Wang, X. Wang, Appl. Surf. Sci. 254 (2008) 1915.
[63] C. van der Marel, M. Yidirim, H.R. Stapert, J. Vac. Sci. Technol., A 23 (2005) 1456.
[64] P.J. Cumpson, Surf. Interface Anal. 31 (2001) 23.
[65] J. Bicerano, Prediction of Polymer Properties, 3 ed. Marcel Dekker, Inc., New York, 2002.
[66] A. Chazan, Peptide Property Calculator, http://www.basic.northwestern.edu/biotools/proteincalc.html(October 14, 2010).